A Novel Grid-demanded Power Point Tracking (GPPT) Control Method for Wind Turbines to Preserve Grid Stability with High Wind Energy Penetration

David Matthies, Alexander Ernst, Henning Sauerland, René Reimann, Wilfried Holzke, Bernd Orlik
IALB, University of Bremen
Otto-Hahn-Allee 1, NW1
D-28359 Bremen, Germany
Tel.: +49 421 218-98 626 92
E-Mail: dmatthies@ialb.uni-bremen.de
URL: https://www.uni-bremen.de/ialb

Keywords

«Wind energy», «Wind-generator systems», «Virtual Synchronous Generator (VSG)», «Test bench», «Smart power»

Abstract

To keep a stable grid operation despite shut-down power plants, wind turbines need to provide equal ancillary services. Therefore, a sophisticated grid-demanded power point tracking (GPPT) control method is proposed. This control strategy was successfully validated on a test bench, so that it may probably run on real wind turbines.

Introduction

In order to finally realize the implementation of the energy transition, large CO_2-emitting power plants need to be adequately replaced by renewable energy sources to a greater extent. Hereby, wind turbines are of central significance [1]. Figure 1 shows a commonly installed wind turbine with a full-scale converter, a permanent magnet synchronous generator (PMSG) and an active pitch control. Conventional control strategies aim at a maximum wind power point tracking (MPPT) without regarding the electrical consumer power demand, whereas a balance between the produced and consumed power actually is one mandatory prerequisite for a stable grid operation. Therefore, the highly grid-stabilizing
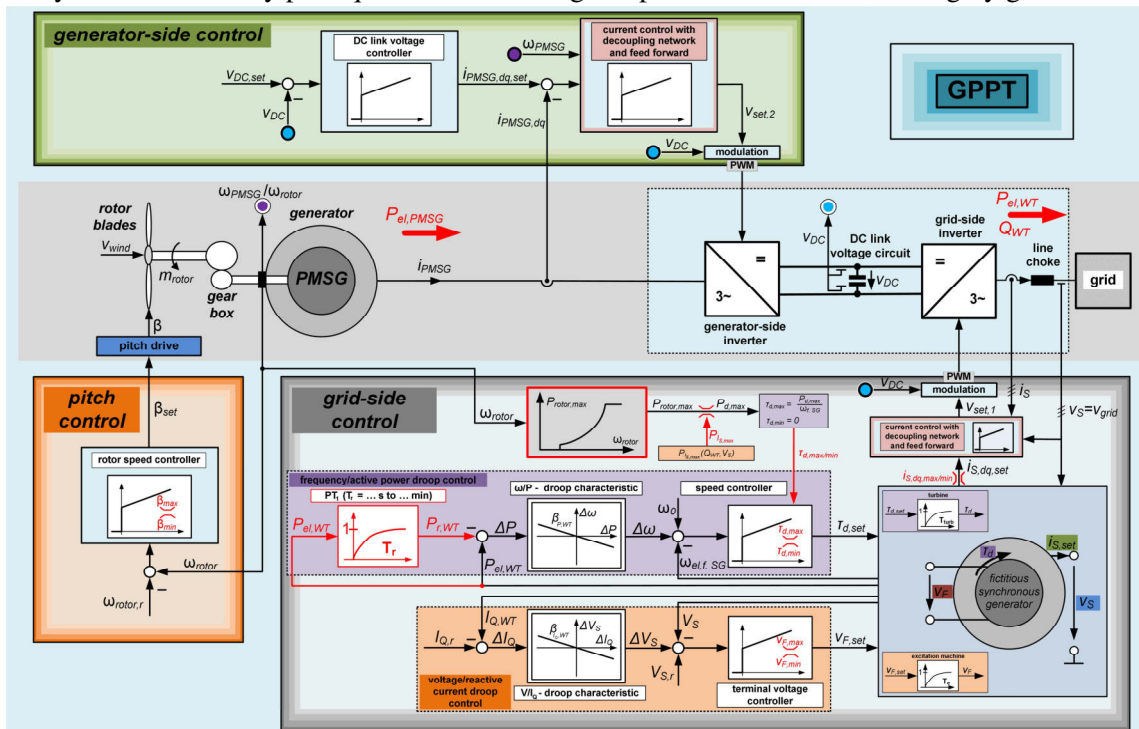

Fig. 1: Developed highly grid-stabilizing GPPT control strategy

wind turbine control strategy of Fig. 1 was developed to make the still indispensable provision of ancillary services by power plants, e. g. in terms of voltage and frequency stability, redundant. Here it must be considered, that current power plant dominated grid processes have to be appropriately adapted to the specific properties of wind turbines such as, inter alia, fast changing unpredictable wind speeds or their huge number with a relatively low power class in each case [2]. Keeping the given wind turbine structure unchanged, the three available control interventions were modified. Hereby, the resulting grid-demanded power point tracking (GPPT) control strategy has to consider all these complicating factors and additionally combine them with power plant behaviour as analogue as possible. Only thus, a reasonable interference in long-proven methods within the complex electricity grid is feasible, so that future grid stability can be sustainably preserved.

Grid-demanded Power Point Tracking (GPPT)

By analogy with conventional power plants and to keep proven physical grid characteristics, the grid-side inverter should behave like a directly grid-connected synchronous generator based on the principle of current synchronverter approaches [3]. Therefore, the used generator model [4] receives the measured terminal voltage v_S as an input value and the resulting set currents $i_{S,set}$ are set by a current control for a generator equivalent power input into the grid, validated in [2]. The fictitious mechanical drive

Fig. 2: Overview of an MPPT control structure

torque τ_d and the excitation voltage v_F serve for the generator control and are set by a turbine and an excitation machine. These are approximated by a respective PT1-element with the time constants $T_{turb} = 50\ ms$ and $T_e = 10\ ms$ [5]. Over this, the implemented frequency/active power droop control with an appropriate drive torque limitation to $\tau_{d,\,max/min}$ and the voltage/reactive current droop control intervene in the grid power flow. Opposed to the conventional MPPT control method of Fig. 2 [1], it is therefore now up to the generator-side inverter to control the DC link voltage v_{DC} cascaded with a subordinate current control [4]. The combination of the fed active power $P_{el,\,WT} = P_{el,\,PMSG}$ with the rotor speed control by pitch angle adjustment specifies the resulting operating points of the wind rotor. For the practical validation, the illustrated test bench with a central control in Fig. 3 was set up [6] to reproduce a wind turbine with real rotor behaviour feeding into an emulated electricity grid. The grid consists of a power plant and a common load to represent a grid state with high wind energy penetration [2] according to Fig. 4. Herein, the chosen wind turbine parametrization is listed as well.
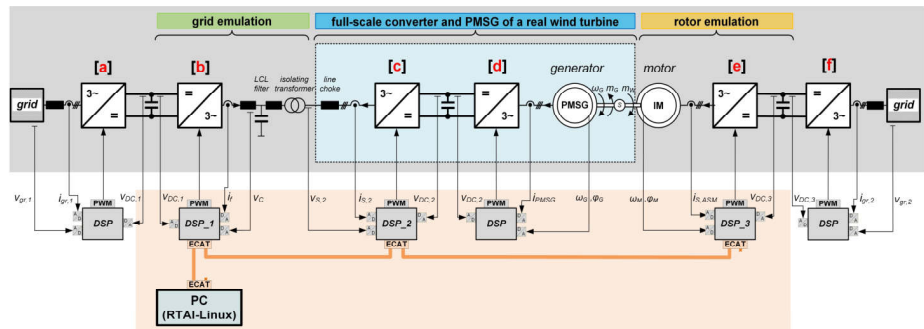

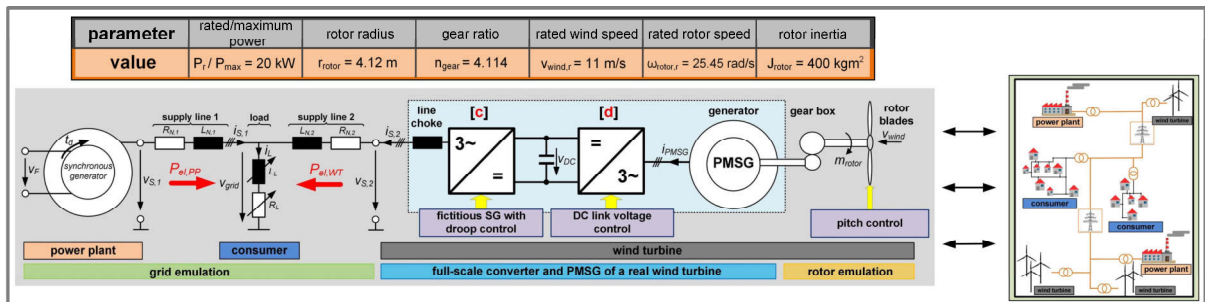Fig. 3: Wind turbine test bench to validate the GPPT control method

Fig. 4: Chosen wind turbine parametrization and desired test bench functionality

Basic Element: Fictitious Synchronous Generator

Figure 5 depicts a single-phase equivalent circuit of the used separately excited synchronous generator (SESG) in Fig. 1 divided up into the rotor and stator circuit with their respective passive components. Here, the excitation voltage v_F adjusts the magnitude and the drive torque τ_d the phase angle of the internal generated voltage v_i [5]. Thereby, the generator active and reactive power is determined.
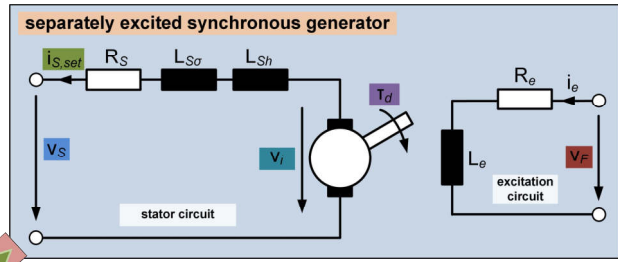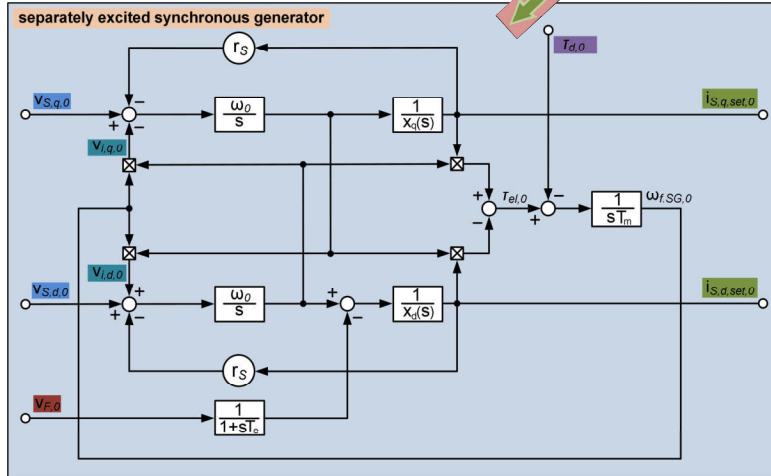

Fig. 5: Equivalent circuit of an SESG

Fig. 6: Applied synchronous generator model [6]

Taking an additional damper winding into consideration, the corresponding applied generator model was derived in [4] and [7] and is shown in Fig. 6 in the d/q reference frame with redefined variable and parameter names.

The developed model requires, that the input and output values are normalized to their related rated values of Table 1, such as e. g. $v_{S,q,0} = \frac{v_{S,q}}{V_{S,r}}$. In accordance to the desired power class, the model variables in Fig. 6 $(x_d(s), x_q(s), \dots)$ can be parametrized by a fitting data sheet. The relevant parameters of it are listed in Table 1 and specify the properties of the synchronous machine. Hereby, equal values for the direct-axis and quadrature-axis synchronous reactances $(x_d = x_q)$ indicate a non-salient pole synchronous generator as mostly applied in power plants. With the chosen inertia time constant $T_m = 100\ ms$ and the resulting electrical torque $\tau_{el,0}$ the dynamic behaviour is described by

$$\omega_{f.SG,0} = \frac{1}{T_m} \cdot \int \tau_{el,0} - \tau_{d,0}\ dt. \quad (1)$$

The damper winding and, therefore, the generator damping behaviour is adjusted by unequal values of the direct-axis transient and sub-transient reactances $(x_d' \neq x_d'')$.

Table 1: Parametrization of the fictitious synchronous generator

general data (rated values):			
apparent power	$S_r = 37.5\ kVA$	power factor	$\cos \varphi_r = 0.8$
phase voltage	$V_{S,r} = 230\ V$	number of pole pairs	$p = 2$
phase current	$I_r = \frac{S_r}{3 \cdot V_{S,r}} = 54.1\ A$	angular frequency	$\omega_0 = 314.15\ \frac{rad}{s}$
resistances:			
stator winding resistance	$R_S = 0.1713\ \Omega$		
reactances (per unit):		**time constants:**	
direct/quadrature -axis synchronous reactance	$x_d = 0.967\ /$ $x_q = 0.967$	direct-axis transient open-circuit time constant	$T_{d0}' = 0.57\ s$
direct/quadrature -axis transient reactance	$x_d' = 0.152$	direct-axis transient short-circuit time constant	$T_d' = 0.024\ s$
direct/quadrature -axis subtransient reactance	$x_d'' = 0.083\ /$ $x_q'' = 0.169$	direct/quadrature -axis subtransient open-circuit time constant	$T_d'' = 0.015\ s\ /$ $T_q'' = 0.015\ s$

The left side of Fig. 7 shows the actual values $i_{S, 2, dq}$ and the set values $i_{S, 2, dq, set}$ (test bench in Fig. 3 referred variable names) of the generator stator currents in the d/q reference frame at a constant terminal voltage $v_{S, 2}$.
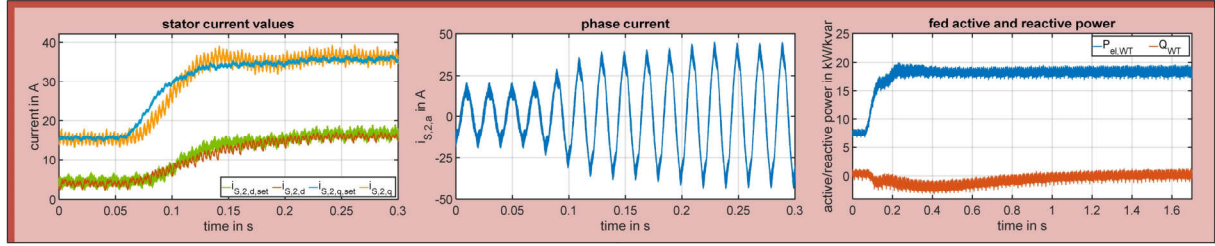

Fig. 7: Set and actual stator current values, phase current and active and reactive power on a torque jump $\Delta\tau_{d, set}$

At about $60\ ms$ a torque jump $\Delta\tau_{d, set, 0}$ of 30 percent of the nominal torque value is performed. The control error reaches zero after several milliseconds, which is sufficiently fast so that the regarded system acts like a real generator. It appeared, that the existing harmonics in the measured stator voltage $v_{S, 2}$ highly affect the set currents $i_{S, 2, dq, set}$ caused by the transmission behaviour of the used generator model (Fig. 6). Therefore, the set currents are additionally filtered with the time constant $T_f = 0.005\ s$. During the measurement in Fig. 7, the fed reactive power Q_{WT} is controlled to zero by adjusting the excitation voltage v_F. Moreover, the resulting fed active power $P_{el, WT}$ and the phase current $i_{S, 2, a}$ are depicted.

Before feeding into the grid it is mandatory, that the generator model synchronizes itself to the grid voltage v_{grid}, given out by inverter [b] (Fig. 3). The short-circuited damper winding behaves similar to the squirrel cage of an induction machine and, therefore, provides a starting torque at standstill. As soon as the measured grid voltage is applied ($v_{S, 2} = v_{grid}$), the fictitious generator runs up to about the grid frequency f_{grid} as shown in Fig. 8 (asynchronous start-up). Then, the synchronous persistence completes the synchronization to $\omega_{el, f. SG} = \omega_{grid}$ and the damper winding has no more influence for the moment.
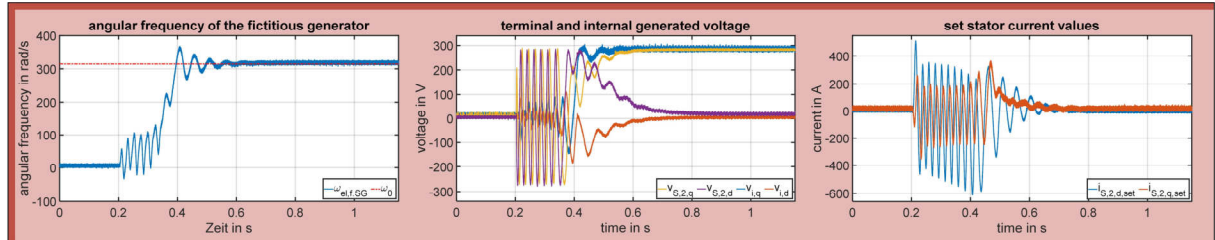

Fig. 8: Synchronization process of the fictitious generator

Because it is not a real machine, high set current values $i_{S, set}$ are absolutely permitted during the synchronization process. But at the time when the wind turbine starts to feed into the grid, these need to be around zero. According to the equivalent circuit in Fig. 5, the internal generated voltage v_i needs to get close to the terminal voltage v_S in order to minimize the voltage drop across the passive components. Therefore, the excitation voltage $v_{F, 0}$ is fed forward by a value of 0.95 and the drive torque is set to $\tau_{d, 0} = 0$. This leads to the courses of the terminal and internal generated voltages of Fig. 8 in the d/q reference frame. After the start-up, the respective d- and q-components are running towards the equal value, which also excludes a possible angular offset. In addition, the resulting set current values $i_{S, 2, dq, set}$ approximate the desired value of zero after synchronization.

Basic Element: Generator-Side Boost Converter

At first, the conventional grid-side boost converter as applied on wind turbines with MPPT control and also on inverter [a] and [f] on the test bench (Fig. 3) is regarded on the left side of Fig. 9.
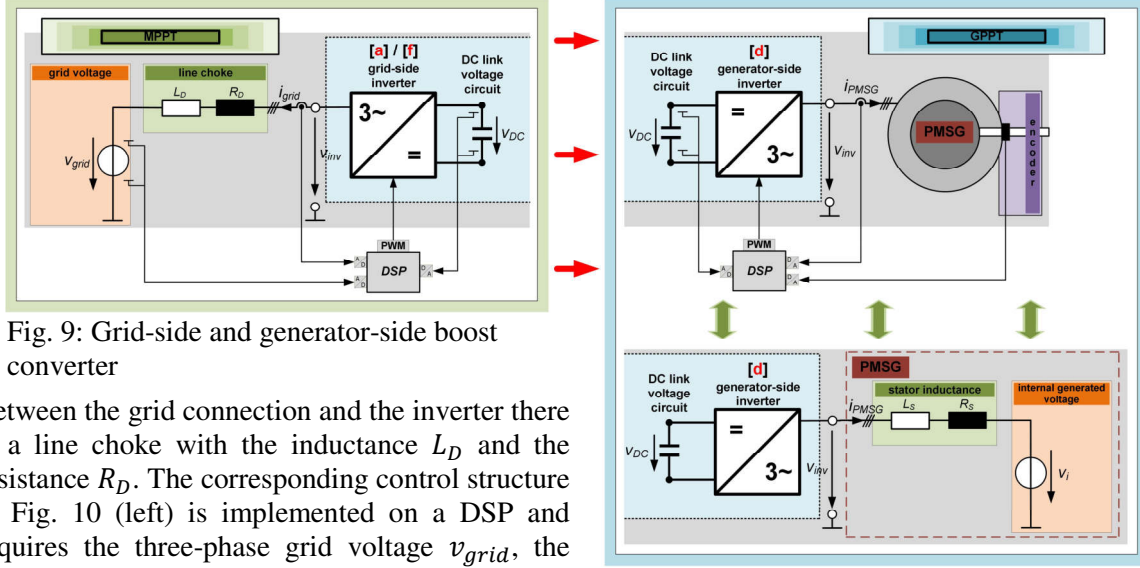

Fig. 9: Grid-side and generator-side boost converter

Between the grid connection and the inverter there is a line choke with the inductance L_D and the resistance R_D. The corresponding control structure in Fig. 10 (left) is implemented on a DSP and requires the three-phase grid voltage v_{grid}, the current i_{grid} and the DC link voltage v_{DC} as the measured input values. To determine the mains angle φ_{grid} needed for the d/q transformation, a phase-locked loop (PLL) is used. The DC link voltage v_{DC} is controlled with a subordinate current control of the active current component $i_{grid,d}$ in the d/q reference frame. The respective current controller output is fed forward by a decoupling network and the grid voltage $v_{grid,d}$ ($v_{grid,q} = 0$ for transformation angle φ_{grid}). Eventually, the PWM signal for the inverter control is generated out of the resulting set voltages $v_{set,dq}$.

Starting from this, the detailed control structure of the generator-side boost converter at GPPT on the right side of Fig. 10 is accordingly adapted for the connected PMSG in Fig. 9 (right).
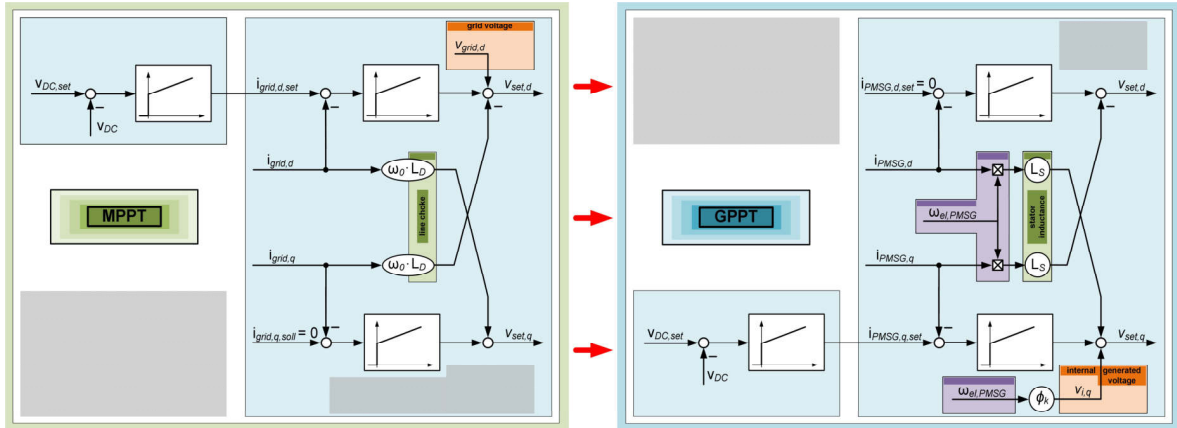

Fig. 10: Comparison between the control structure of a grid-side and generator-side boost converter

The relevant parameters of the PMSG are listed in Table 2. The related depicted equivalent circuit in Fig. 9 (right) directly emphasizes the analogy between both concepts. Hereby, the stator impedance (L_S and R_S) is comparable to the line choke (L_D and R_D) and the internal generated voltage v_i represents the grid voltage v_{grid}. In contrast, due to the applied electrical machine, $i_{PMSG,q}$ now represents the active current component subordinated to the DC link voltage controller. Moreover, the fed forward internal generated voltage $v_{i,q}$ hence affects the q-component. Opposed to the

Table 2: Parameters of the applied PMSG

parameter	value
rated power	$P_{r,PMSG} = 30\ kW$
rated speed	$\omega_{PMSG,r} = 104.72\ \frac{rad}{s}$
rated terminal voltage	$V_{S,PMSG,r} = 230\ V$
number of pole pairs	$Z_p = 3$
stator inductance	$L_S = 20\ mH$

measurable grid voltage v_{grid}, $v_{i,q} = \phi_k \cdot \omega_{el,PMSG}$ is determined by the known constant magnetic flux $\phi_k = \frac{\sqrt{2} \cdot V_{S,PMSG,r}}{Z_p \cdot \omega_{PMSG,r}} = 1.035\ Wb$ and the generator speed $\omega_{el,PMSG} = Z_p \cdot \omega_{PMSG}$. The speed is calculated out of the generator rotor angle φ_{gen} output by the encoder which is now also used for the d/q transformation. Contrary to the nearly constant grid frequency $\omega_0 = 2\pi \cdot 50\ Hz$, a variable generator speed range is resulting and, therefore, needs to be considered in the decoupling network as an input value.

Hereto, Fig. 11 shows a measurement for a linearly increasing generator speed ω_{PMSG} from $\frac{\omega_{PMSG,r}}{2}$ to $\omega_{PMSG,r}$ with an applied load of $\Delta P_{el,WT} = 7.5\ kW$ or rather $\Delta \tau_{d,set,0} = 0.2$ at the time $t = 4\ s$ by the fictitious generator. The DC link voltage v_{DC} is kept within an acceptable value range during the whole speed change and the phase current $i_{PMSG,a}$ is adapted to the increased power demand.
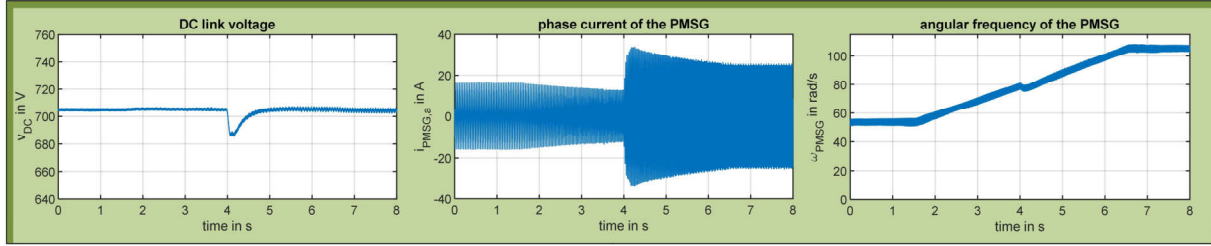

Fig. 11: Related measurement results of the DC link loaded during a speed change
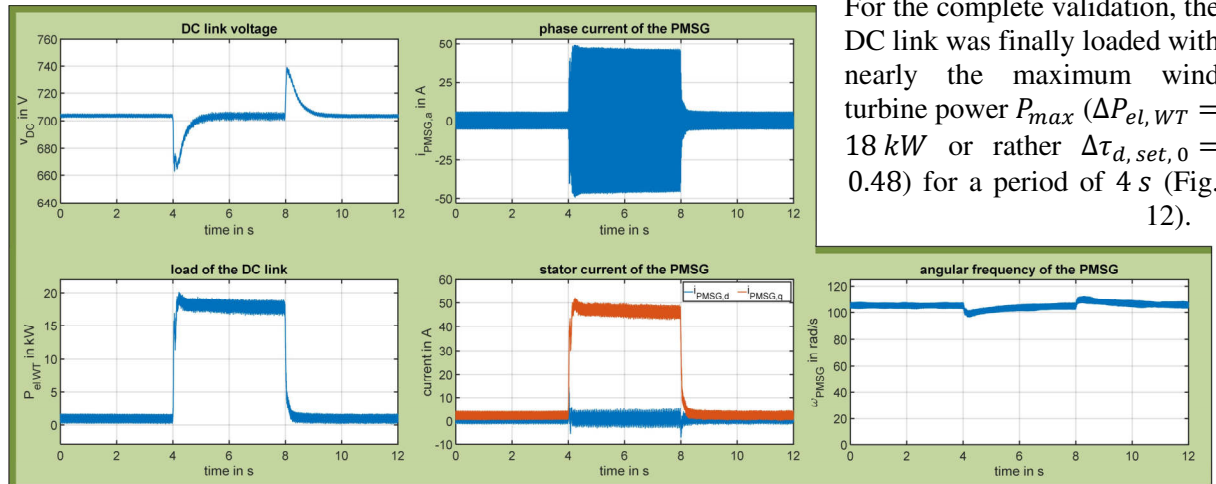

For the complete validation, the DC link was finally loaded with nearly the maximum wind turbine power P_{max} ($\Delta P_{el,WT} = 18\ kW$ or rather $\Delta \tau_{d,set,0} = 0.48$) for a period of $4\ s$ (Fig. 12).

Fig. 12: Measurement results of the DC link loaded with the nearly maximum wind turbine power

Active Power Flow

Whereas the always ensured availability of fossil fuels allows a power plant design with a constant rated power $P_{r,PP}$, wind turbines hereby encounter problems with fast unpredictable wind speeds. Therefore, the rated power $P_{r,WT}$ of the wind turbine is now directly shifted from the resource wind to the demanded power of the consumer by assuming it as the delayed fed-in power $P_{el,WT}$ (Fig. 1) [2], [8]. When a load change ΔP_{load} occurs (Fig. 4), the additional demanded power is extracted from the respective kinetic energy of the rotating generator inertia at first (instantaneous reserve). Then, the frequency/active power droop control provides a coordinated and defined load distribution between the power plant (PP) and the wind turbine (WT) according to Fig. 13 (primary reserve). The time constant T_r defines the time it takes for the frequency set value $\omega_{set,WT} = \omega_0 + \beta_{P,WT} \cdot (P_{el,WT} - P_{r,WT})$ to reach the nominal grid frequency

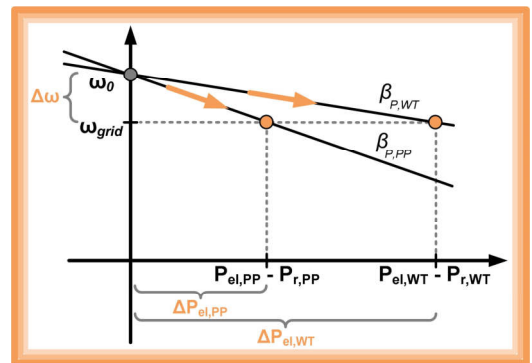Fig. 13: Defined load distribution

ω_0. Meanwhile, the consistent grid frequency ω_{grid} forces the wind turbine to additionally take over the whole reserve power of the power plant so that it returns to its rated power $P_{r,PP} = P_{el,PP} = 40\ kW$ as well (Fig. 14, time range from 0 to 110 s and 195 s to 360 s for $T_r = 6\ s$).

Hence, the wind turbine even behaves like a regulating power plant and restores ω_0 as long as there is enough extractable wind power $P_{rotor,max}$ available. Otherwise, the settable fictitious mechanical drive torque $\tau_{d,set}$ is appropriately limited making use of the known wind turbine power curve $P_{rotor,max}(\omega_{rotor})$ in Fig. 1 originally developed for MPPT control:

$$\tau_{d,min} = 0 \text{ and } \tau_{d,max} = \frac{P_{d,max}}{\omega_{f.SG}} \tag{2}$$
$$\text{for } P_{d,max} = P_{rotor,max}.$$

Without any wind speed measurement, the wind turbine can now pass through its whole power range and directly aim towards the value leading to the best load-demanded power flow:

$$0 \le P_{el,WT} \le P_{rotor,max}. \tag{3}$$

The grid feed-in of Fig. 14 requires, that the DC link voltage v_{DC} is kept constant to a value of 700 V by the generator-side control, validated in Fig. 15.
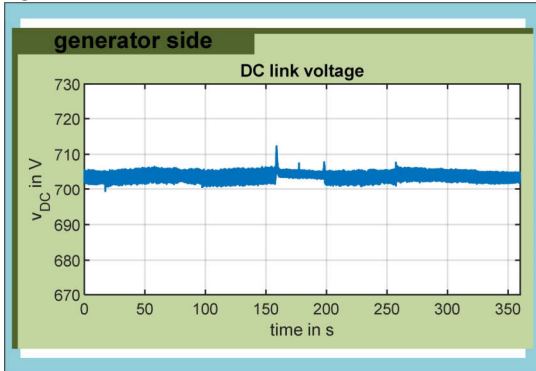

Fig. 14: Load distribution between PP and WT and resulting grid frequency

Fig. 15: DC link voltage course for the grid feed-in of Fig. 14

According to Eq. (3), the load-dependent generator power $P_{el,PMSG} = P_{el,WT}$ now also leads to a changed value range of the resulting rotor-side referred electrical generator torque $m'_{el,PMSG}$ (Eq. (4)) compared to a conventional MPPT control method ($P_{el,PMSG} = P_{rotor,max}$). Equation (4) determines, that the rotor speed ω_{rotor} varies until the wind-induced rotor torque m_{rotor} equals $m'_{el,PMSG}$.

$$J_{rotor} \cdot \dot{\omega}_{rotor} = m_{rotor} - m'_{el,PMSG}$$
$$\text{with } m'_{el,PMSG} = \frac{P_{el,PMSG}}{\omega_{rotor}} \cdot n_{gear} \text{ and } m_{rotor} = \frac{P_{rotor}}{\omega_{rotor}} \tag{4}$$

Then, a stationary state is achieved and the resulting wind rotor operating points rotor speed ω_{rotor}, pitch angle β and power coefficient c_p are defined. Hereby, c_p describes the ratio between the extracted amount of rotor power P_{rotor} and the total available wind power P_{wind} with the rotor radius r_{rotor} and wind speed v_{wind}:

$$c_p = \frac{P_{rotor}}{P_{wind}} \text{ with } P_{wind} = \frac{1}{2} \cdot \rho_0 \cdot \pi \cdot r_{rotor}^2 \cdot v_{wind}^3. \tag{5}$$

On the rotor specifying wind power coefficient characteristic of Fig. 16, the coefficient c_p is plotted over the tip speed ratio $\lambda = \frac{\omega_{rotor} \cdot r_{rotor}}{v_{wind}}$ for different pitch angles β.

Depending on the demanded power P_{load} of the consumer, a possible wind rotor operating range occurs to accordingly extract the current fed power $P_{el, WT} = P_{rotor}$ from the wind [8]. At full load operation, the maximum available rotor power $P_{rotor, max}$ is limited to P_{max} and specified by

Fig. 16: Wind power coefficient characteristic with plotted operating points at full and partial load operation

$c_p(\lambda_r)$ at rated rotor speed $\omega_{rotor, r}$, whereas at partial load the wind rotor maximum operates at $(\lambda_{opt}|c_{p, max})$. Here, the rotor power P_{rotor} can only be increased by pitch angle adjustment till the minimum pitch angle $\beta_{min} = 2°$ is set. Therefore, the manipulated variable β of the rotor speed controller is limited to this value. Afterwards, the rotor is braked until at most $(\lambda_{opt}|c_{p, max})$ making use of the favourable aerodynamic effect, that the braking process itself directly implies an increasing wind power extraction [8]. Some resulting power coefficients c_p are exemplarily shown in Fig. 16 for two different assumed load changes $\Delta P_{load, 1}$ (marked with "x") and $\Delta P_{load, 2}$ (marked with "o") at six wind speeds $v_{wind, i}$ with the marked tip speeds ratios $\lambda_{r, i} = \frac{\omega_{rotor, r} \cdot r_{rotor}}{v_{wi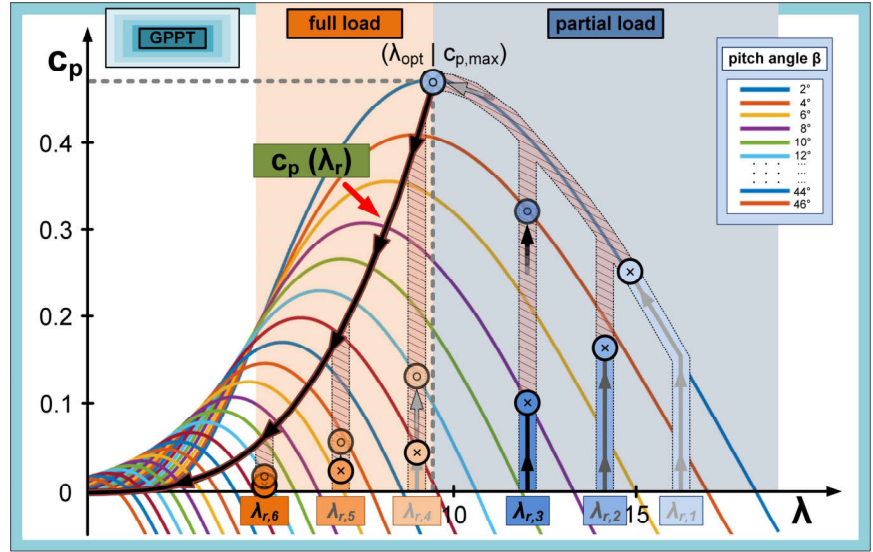nd, i}}$ at rated rotor speed $\omega_{rotor, r}$. These operating points are separately illustrated for β, ω_{rotor} and P_{rotor} over wind speed v_{wind} in Fig. 17 to underline the resulting operating area unlike in MPPT control with only maximum wind power extraction.
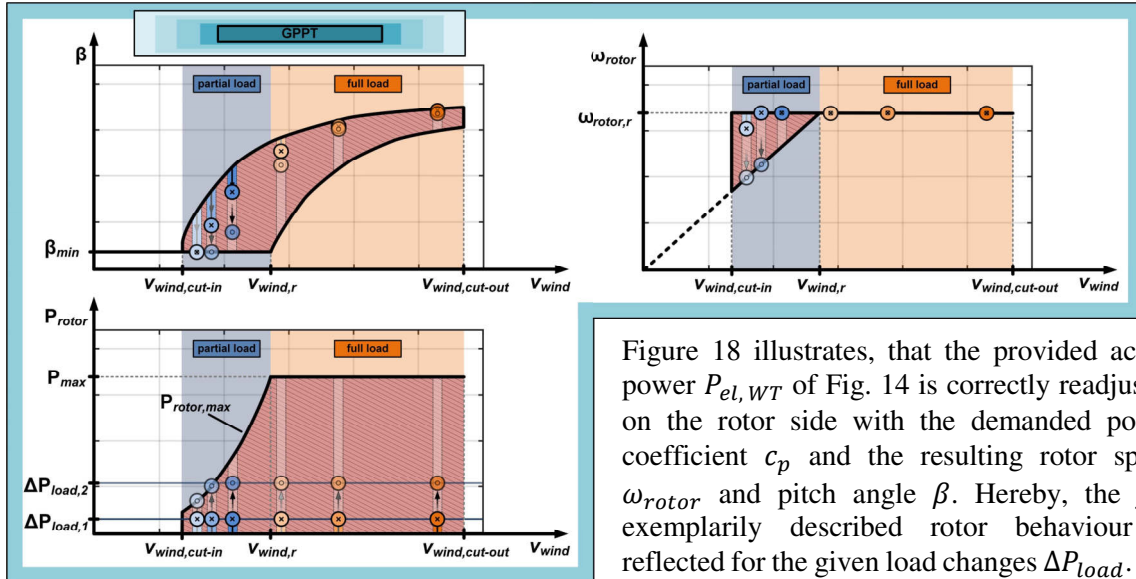

Fig. 17: Separated operating points of Fig. 16

Figure 18 illustrates, that the provided active power $P_{el, WT}$ of Fig. 14 is correctly readjusted on the rotor side with the demanded power coefficient c_p and the resulting rotor speed ω_{rotor} and pitch angle β. Hereby, the just exemplarily described rotor behaviour is reflected for the given load changes ΔP_{load}. For instance, the rated rotor speed $\omega_{rotor, r}$ is kept during partial load operation with $v_{wind} = 8.5 \frac{m}{s}$ from 310 to 360 s.
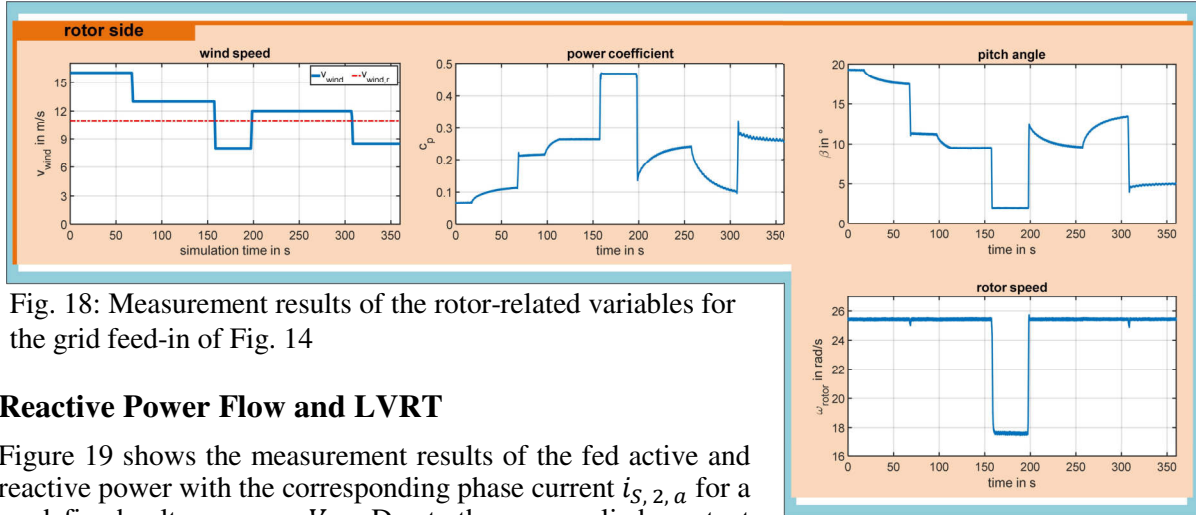
Fig. 18: Measurement results of the rotor-related variables for the grid feed-in of Fig. 14

Reactive Power Flow and LVRT

Figure 19 shows the measurement results of the fed active and reactive power with the corresponding phase current $i_{S,2,a}$ for a predefined voltage course $V_{S,2}$. Due to the now applied constant fixed grid frequency $f_{grid} < f_0$, the frequency/active power droop control then ensures, that the maximum drive power is fed into the grid ($P_{el,WT} = P_{d,max}$). According to the voltage/reactive current droop control [9], the fed reactive power Q_{WT} stays above the rated reactive power $Q_{r,WT} = 4048\ var$ for $V_{S,2} < (V_{S,r} = 230\ V)$ and also vice versa. If necessary due to the decreased terminal voltage, the implemented active power reduction with $P_{d,max} = P_{I_{S,max}}$ intervenes to keep $i_{S,2,a}$ at the permitted inverter maximum current of $\hat{I}_{S,max} = 47\ A$ unless $P_{d,max} = P_{rotor,max}$ (Eq. (2)) becomes effective in case of an occurring wind power drop (time range from 270 to $300\ s$).

Figure 20 shows the wind turbine riding through a voltage course $V_{S,2}$ according to the technical requirements in [9] ($V_{S,VLC}$ with an extended time range to fully set Q_{WT} defined by the droop control in the temporal size of power plants) without disconnecting from the grid (LVRT). Due to the now higher voltage gradients, an additional limitation of the fictitious generator set current values $i_{S,dq,set}$ to the constant values $i_{S,dq,max/min}$ is applied (Fig. 1) to avoid an otherwise resulting phase over current $i_{S,2,a} \geq \hat{I}_{S,max}$.
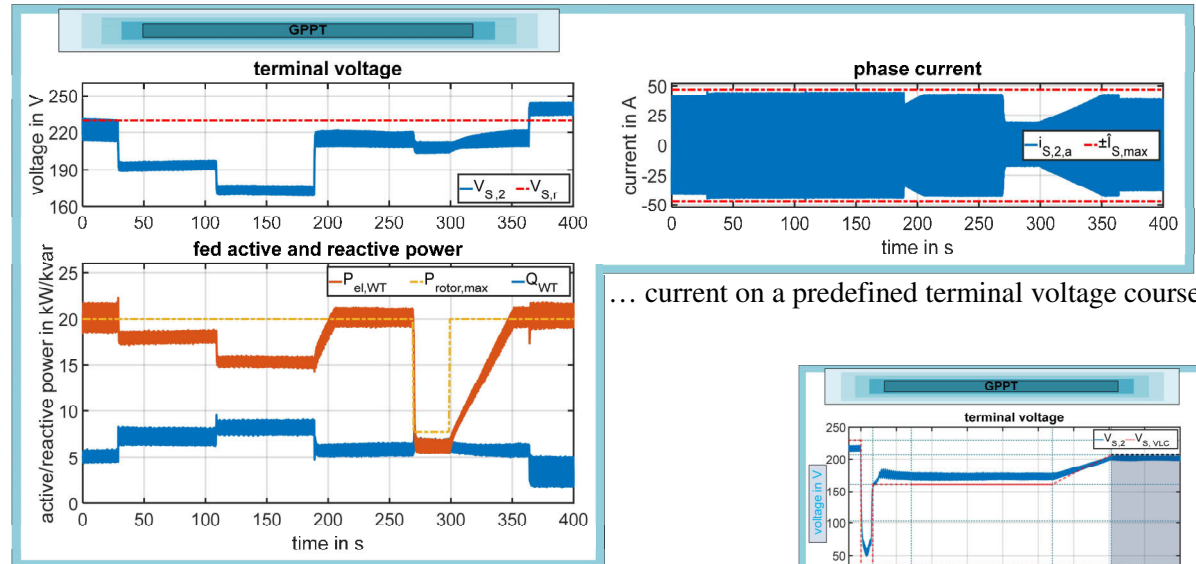

… current on a predefined terminal voltage course

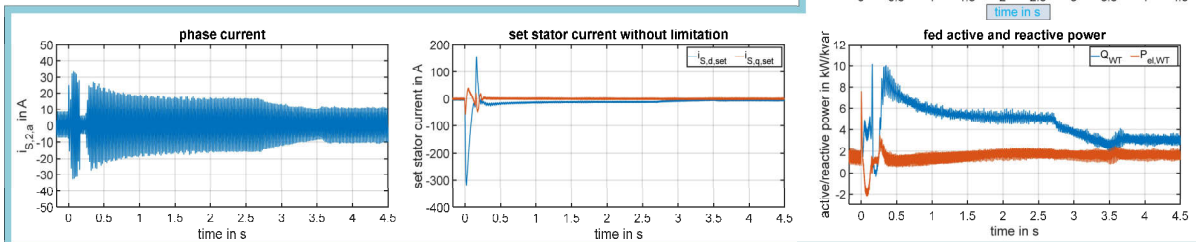Fig. 19: Resulting active and reactive power and phase …

Fig. 20: Effectiveness of set current limitation on a predefined voltage course (LVRT)

Conclusion

Assuming wind energy as the most promising alternative to conventional power plants, a modified grid-stabilizing wind turbine control strategy called grid-demanded power point tracking (GPPT) was developed. Hereby, its basic elements as the applied fictitious synchronous generator and the generator-side boost converter and furthermore the control method as a whole were successfully validated on a test bench built up for this purpose. It has been proven, that equally to conventional power plants, the wind turbine provides the relevant operating reserves needed for a stable grid operation. Reconciling the two independent values wind and load profile, the wind turbine adapts its output power to the consumer and appropriately readjusts it on the rotor side. Moreover, the wind turbine fulfils grid supporting tasks and even performs LVRT. For this reason, the application of GPPT control could be suitable to become independent of the still indispensable ancillary services of power plants.

References

[1] J. Thongama and M. Ouhrouche, „*MPPT Control Methods in Wind Energy Conversion Systems*", chapter in book: Fundamental and Advanced Topics in Wind Power, 2011

[2] D. Matthies, A. Ernst and B. Orlik, „*Wind Energy Powered Electricity Grids*", in PCIM Europe digital days, Germany, 2020

[3] Q. Zhong and G. Weiss, „*Synchronverters: Inverters That Mimic Synchronous Generators*", in IEEE Transactions on Industrial Electronics, 2010

[4] A. Ernst, D. Matthies, W. Holzke and B. Orlik, „*Validation of a Generator-Side Boost Converter with Load by a Fictitious Synchronous Machine*", in PCIM Europe digital days, Germany, 2021

[5] W. Leonhard, „*Regelung in der elektrischen Energieversorgung*", Stuttgart: Teubner Studienbücher, 1980

[6] D. Matthies, W. Holzke, R. Reimann and B.Orlik, „*Practical Validation of a New Control Strategy for Wind Turbines by the Use of a Central PC for Model Calculation*", in PCIM Europe, Nuremberg, Germany, 2019

[7] H. Bühler, „*Einführung in die Theorie geregelter Drehstromantriebe*", Springer Base AG, 1977

[8] D. Matthies, A. Ernst, S. Sauerland, R. Reimann, W. Holzke and B. Orlik, „*Provision of Power Plant Equal Ancillary Services by Wind Turbines: From Maximum to Grid-demanded Power Point Tracking*", in PCIM Europe, Nuremberg, Germany, 2022

[9] TenneT TSO GmbH „*Netzanschlussregeln – Hoch- und Höchstspannung –*", 2015